Journal of Materials Chemistry A

PAPER

View Article Online
View Journal | View Issue

Self-healing mechanisms of water triggered smart coating in seawater†

Cite this: J. Mater. Chem. A, 2014, 2, 1914

Wei Wang,*[ab] Likun Xu,[a] Xiangbo Li,[a] Zhifeng Lin,[a] Yi Yang[ac] and Enpeng An[ac]

Received 27th August 2013
Accepted 23rd October 2013

DOI: 10.1039/c3ta13389c

www.rsc.org/MaterialsA

Scratched alkyd varnish coating (AVC), with isophorone diisocyanate (IPDI) microcapsules as functional additives, display self-healing properties. Here we investigated the mechanism of the self-healing process using a water trigger in seawater. Electrochemical impedance spectroscopy was used to monitor the self-healing efficiency. A detailed examination of the penetration of seawater into the crevice, the self-healing process along the crevice, the self-healing process of seawater penetrating into the coating and failure process of the coating was carried out. The self-healing time of IPDI-AVC was influenced by different metal substrates and self-healing could be inhibited by active metals such as Q235 steel. Due to the formation of a thin metal-oxide layer on the metal surface, other metals, such as 5083 aluminum alloy, titanium and copper, had much less influence on the self-healing time of IPDI-AVC. This study enhances the comprehension of the mechanism of self-healing AVC functionalized by the addition of microcapsules.

Introduction

Recently, microcapsule-type coatings have received increased attention due to their excellent and highly efficient self-healing properties, large healing material quantities, thermal stability and variability of possible triggers.[1] Self-healing processes need additional environmental stimuli as triggers, such as heat,[2] irradiation,[3] mechanical induction,[4] ion concentration,[5] triggering groups[6] and so on.

In the first generation of self-healing microcapsules, poly(urea-formaldehyde) microcapsules were used to encapsulate endo-dicyclopentadiene that acted as a liquid healing agent *via* an *in situ* polymerization in an oil-in-water emulsion. These were mixed with Grubbs' catalyst embedded in an epoxy matrix and together, formed a self-healing coating that used physical cracking as the trigger.[7] The self-healing process was triggered by a crack-induced rupture of the embedded capsules. Then, other kinds of self-healing materials were synthesised for a prolonged, or a controllable, self-healing of the active species on demand, such as silica nanocontainers,[8] sunlight-induced self-healing protective coating,[9] pH-responsive hydrogel,[10] double-layer microcapsules,[11] and a chitosan reservoir of corrosion inhibitor.[12]

Since isocyanates are water-sensitive, their use as an additive can greatly extend the potential catalyst-free healing properties of self-healing materials that are exposed to moist or wet environments. For example, some self-healing coatings used isophorone diisocyanate (IPDI) and hexamethylene diisocyanate (HDI)[13] as healing agents that were encapsulated *via* the interfacial polymerization reaction of diisocyanate prepolymer and 1,4-butanediol in an O/W emulsion.

Most recently, a new self-healing architecture was introduced that mimics human skin and is based on an epoxy coating/substrate architecture. Using dual interpenetrating microvascular networks in such self-healing materials can hold two-component healing chemistries that enable repeated healing of damage in a localized region.[7b] However, the preparation of microvascular networks is complicated, and current microvascular networks display a large dimension[14] and low network resolution that is not suitable for coating applications.

Typical tests to characterize self-healing properties of coatings include tensile testing experiments,[14] morphology characterization,[7b] and rheological evaluation.[15] Unfortunately, as large scale test methods, these offer no *in situ* information about the self-healing process. Electrochemical impedance spectroscopy (EIS) and the scanning vibrating electrode technique are therefore used to characterize the healing ability of coatings.[16] These can also be utilized to evaluate the healing behavior of inhibitor microcapsules using different dipping times.[17]

In our previous work, we reported the synthesis of IPDI and HDI microcapsules through *in situ* polymerization and the improvement of their micromechanical behavior.[18] Here, we present a self-healing system capable of autonomously

[a]State Key Laboratory for Marine Corrosion and Protection, Luoyang Ship Material Research Institute (LSMRI), 149-1 Zhuzhou Road, Laoshan District, Qingdao 266101, P. R. China. E-mail: wwei020404@126.com

[b]College of Materials Science and Chemical Engineering, Harbin Engineering University, Harbin 150001, P. R. China

[c]State Key Laboratory of Advanced Technology for Materials Synthesis and Progressing, Wuhan University of Technology, Wuhan 430070, P. R. China

† Electronic supplementary information (ESI) available: Experimental details of synthesis microcapsules and plasma treatment. See DOI: 10.1039/c3ta13389c

repairing repeated damage events. A self-healing mechanism model of scratched IPDI-AVC immersed in seawater was established. The IPDI-AVC showed self-healing properties when coated on 5083 aluminum alloy, titanium, copper and Q235 steel surfaces. Self-healing time is modified by the activity of metals. Self-healing properties of IPDI-AVC also depended on the width of the crevice.

Experimental section

Materials

All chemicals were obtained from Sigma Aldrich. Water used in all experiments was purified by a Millipore Milli-Q Plus 185 purification system with a resistivity higher than 18.3 MΩ cm. All metals used in the experiments were purchased from Shanghai BaoSteel. The purity of the copper was at least 99.99%. Alkyd varnish was purchased from Lehua Inc. China. Air dry alkyd varnish consisted of solvent naphtha and alkyd resin. The drying process of the alkyd varnish includes solvent evaporation, hydroperoxide formation, hydroperoxide decomposition into free radicals, and polymerisation.[19] All chemicals were used as received.

Characterization

The conductivity (4.863 S m^{-1}) and pH (7.36) of the seawater were measured using a YSI 6600 (YSI Inc). Plasma treatment tests were carried out using a Model EPPs 2000, Plasmart Inc. China. Scanning electron microscopy (SEM) images of the samples were acquired with a XL30 ESEM microscope. Optical microscopy images were recorded with a VHX-1000, KEYENCE Co., Ltd. Thermogravimetric analysis (TGA) data were obtained from a TGA Q5000, TA Instrument. The glass transition temperature (T_g) of the coating was measured by DSC Q2000, TA Instrument. Fourier Transform Infrared Spectroscopy (FT-IR) tests were performed on a Thermo Scientific Nicolet iN10, Thermo Fisher Scientific Inc. The EIS curves were recorded by an EG&G 2273 potentiostat using AC signals of 20 mV amplitude, peak to peak at an open circuit potential (OCP) in the frequency range of 10^5 Hz to 0.01 Hz, with 42 points. EIS measurements were carried out in a conventional three-electrode cell with a platinum counter electrode and a saturated calomel electrode (SCE) as the reference. All the potentials in this paper are reported in the SCE scale. The volume of the cell was 2000 ml. The specimen was immersed in seawater and allowed to attain a stable OCP before starting the frequency scan. All the tests were performed at 30 °C. ZSimpWin software was used to analyze the EIS data with the equivalent circuit. The measurements of the potential distribution on the steel surface were recorded by the scanning micro-reference electrode (SMRE) technique using a model CSPM5500-XMU-BY Being Nano-Instruments (Beijing, China) device.

Sample preparation

IPDI microcapsules were synthesised through *in situ* polymerization using a modified literature process,[23] as described in the ESI.† The morphology of the IPDI microcapsules is shown in Fig. 1a.

We treated IPDI microcapsules with oxygen plasma. IPDI microcapsules, with surfaces that are modified with hydroxyl, carboxyl, and carbonyl groups, might have a perfect dispersion into the AVC.[18,20] Then, a self-healing corrosion resistant coating was prepared by mixing 16 wt% plasma treated IPDI microcapsules into the AVC. This coating was used to coat the metal surface (Fig. 1b). All coatings with a thickness of 300 μm were applied to a 10 mm × 10 mm metal substrate, and solidified at 40 °C for 72 h. Coating solutions were applied to one end of the substrate, and a micrometer-controlled surgical blade was used to spread the coating to a uniform-thickness.

The IPDI used here was a mixture of Z-IPDI and E-IPDI isomers.[21] The solidification of the self-healing materials produced in seawater was followed by the reaction shown in Scheme 1. R–NCO is the abbreviation of the IPDI chemical formula in Scheme 1. The reaction of IPDI with water decomposes it into a primary amine (product 3 in Scheme 1). Then, the primary amine reacts with the remaining IPDI to yield the product 4 in Scheme 1. After continuous polymerization, polyurethane was obtained.[22]

The reaction of IPDI (2.0 g) and water (2.0 g) in air were performed with mechanical stirring at 30 °C. The mixture became a white solid product after a 12 h reaction (Fig. 2).

Results and discussion

Thermogravimetric analysis

The T_g of the AVC is 4.42 °C. The thermal stability of AVC, and AVC with IPDI, was measured by thermo-gravimetric analysis (TGA). Each sample was examined under nitrogen flow (35 ml min^{-1}) on a TGA Q5000 apparatus at a healing rate of 10 °C min^{-1}

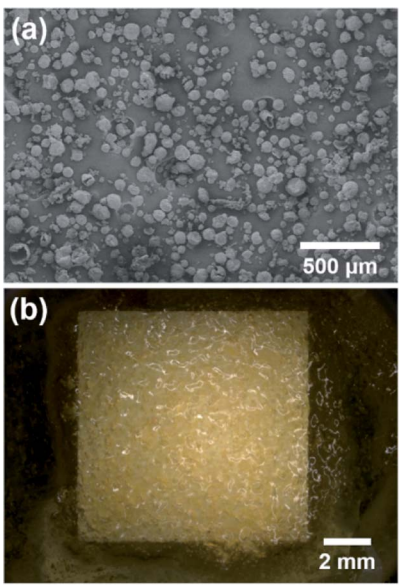

Fig. 1 IPDI microcapsules synthesized *via* an *in situ* polymerization procedure (a) and IPDI-AVC on a 5083 aluminum substrate (b).

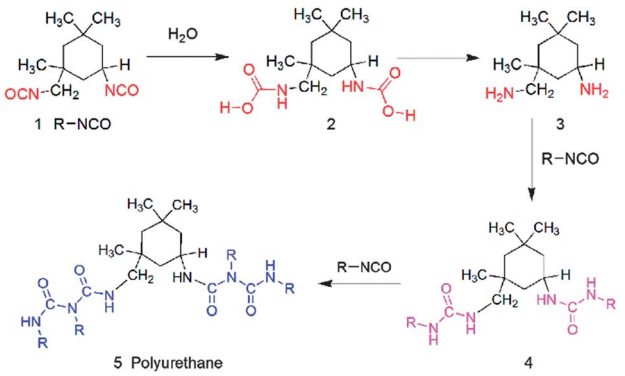

Scheme 1 Schematic representation of the self-healing reaction of IPDI in seawater.

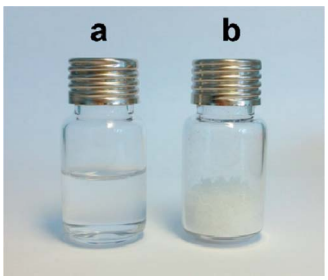

Fig. 2 Photograph of the IPDI (a) and polyurethane (b).

from 25 to 550 °C. The weight of all samples was kept within 4–9 mg in a platinum crucible.

Fig. 3 shows the mass loss curves of IPDI, microcapsule, microcapsule shells, AVC, and AVC with different mass contents of IPDI microcapsules, over the temperature range of 25 to 550 °C. The onset temperatures for loss of mass of AVC and AVC + 16% IPDI microcapsules were 319.7 °C and 321.5 °C, respectively. The TGA tests indicated that the incorporation of IPDI microcapsules into the AVC had little influence on the thermal stability of AVC.

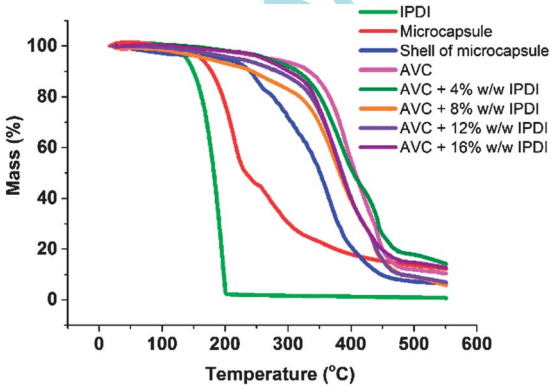

Fig. 3 The mass loss curves of IPDI, microcapsule, microcapsule shells, AVC and AVC with different mass content of IPDI microcapsules over the temperature range of 25 to 550 °C.

Fracture tests

After preparation of IPDI-AVC specimens described previously, rectangle mode IPDI-AVC samples were made. All fracture specimens were tested under displacement control using pin loading and a 5 μm s^{-1} displacement rate. Samples were tested to failure, and the compliance and peak load were measured.

A series of stress–strain experiments were carried out to examine mechanical enhancement by incorporation of the IPDI microcapsules into the healable matrix in Fig. 4. Addition of self-healing microcapsules into the matrix resulted in a dramatic increase of tensile strength of the coating from *ca.* 0.5 MPa for the neat matrix to *ca.* 1.8 MPa for the AVC with 16 wt% microcapsules. The tensile test proved that IPDI microcapsules significantly increased the load of the AVC. Thus, the AVC added with IPDI microcapsules became more brittle and less viscose than pure AVC.[23]

Self-healing morphology

The flat part in Fig. 5 denoted by the yellow outline, shows solidified core healing materials (polyurethane), which flow from the core into the crevice, where they solidify. The microcapsule products in the crevice might have been produced when microcapsules were exposed to moist air or water in storage. After water-triggered solidification of the IPDI, the solid polyurethane was produced (yellow rectangle in Fig. 5), which acted as the final self-healing material to fill the gap or crevice in the coating. The yellow flat part proved that the IPDI microcapsules had a self-healing ability when exposed to moist air or water.

The IPDI-AVC had a thickness of 300 μm. After the self-healing was completed along the crevice path, solidified core healing materials filled the gap. Additionally, some microcapsules near the crevice swelled due to contact with seawater. Fig. 6 shows that the crevice is covered by microcapsules after prolonged immersion in seawater.

The self-healing process only occurred when the self-healing materials were exposed to water as the trigger, without other trigger conditions. The microcapsules easily swelled upon water exposure.[3,24] Swelling of microcapsules due to water permeation created cracks on the surfaces of the microcapsules. This phenomenon is similar to the micro-cracks as shown in Fig. 5. This allowed self-healing materials to flow out of the microcapsules across the crevices and solidify after contact with seawater.

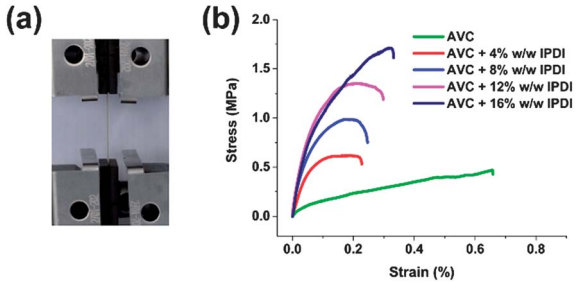

Fig. 4 (a) Photograph of a sample during the fracture test. (b) Stress–strain curves of samples loaded with different contents of IPDI microcapsules in the AVC.

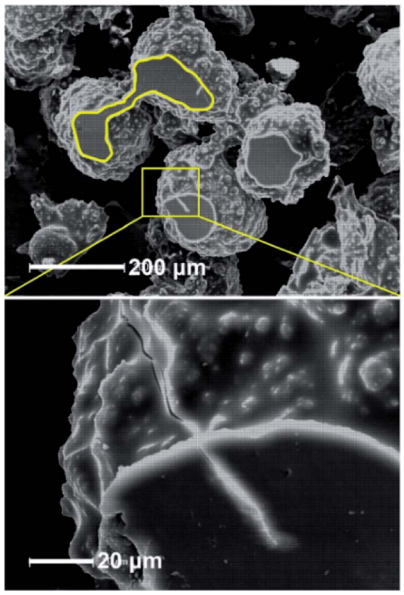

Fig. 5 SEM images of swollen IPDI microcapsules.

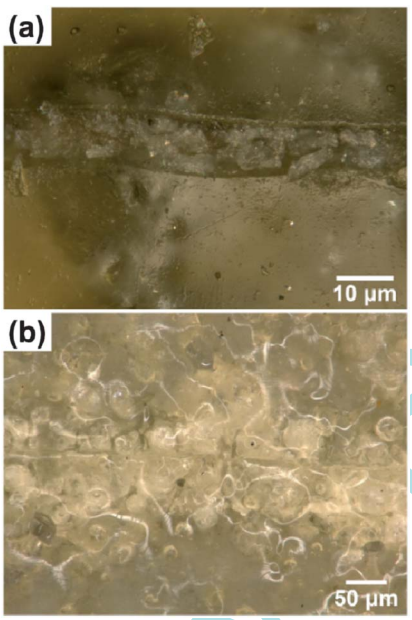

Fig. 6 The crevice of the AVC on the 5083 aluminum substrate is filled with self-healing materials after immersion in seawater for 200 h (a) and 1200 h (b).

If the width of the crevice was >30 μm, no self-healing process occurred in a given time. Therefore the surface was subjected to a narrow scratch of an average width of 10 μm as the starting condition of the self-healing process examinations. Fig. 7 shows that the efficiency of the self-healing process depended on the width of the scratch and the number of consecutive scratches in the same area. Area (I) was subjected to a single scratch 10 μm in width. It healed well after 30 days in seawater. Area (II) and (IV) were subjected to two consecutive scratches of 10 μm width and were well healed after 30 days, showing the ability to self-heal after repeated scratches. Area (III) was subjected to a wider scratch of 30 μm crevice width. After immersion in seawater for 30 days, it still showed a large unhealed scratch. There was not enough healing material available to fill the gap of the scratch. Thus, wider scratch crevices can leave the metal surface susceptible to corrosion. Moreover, the wider crevice could allow seawater to wash away the self-healing materials before the healing reaction is completed. Taken together, the self-healing effect is influenced by the width of the crevice, where self-healing materials flowing out of the microcapsules were able to fully fill narrow scratches, but were not able to do so in wider scratches.

FT-IR spectra

FT-IR spectra of the self-healing materials in the scratched crevice in Fig. 6 show peaks for the isocyanate group (–NCO) at 2263 cm^{-1} and 1337 cm^{-1} in Fig. 8. New bands due to the formation of urea groups appeared at 1637 cm^{-1} (C=O stretching in urethane) and 1560 cm^{-1} (N–H bending in urea) (Fig. 8c). FT-IR spectrum of the AVC shows a peak at 1731 cm^{-1} that also exist in the crevice in Fig. 8c. This identifies that the scratched crevice is cured by IPDI microcapsules.

SMRE characterization

The scanning micro-reference electrode (SMRE) technique was used to monitor the self-healing process of IPDI-AVC (~20 μm thickness) by *in situ* imaging of the corrosion potential with good time and spatial resolutions.[25] After scratching the AVC surface, potential fields are measurable in the solution because of the exposure of the metal surface to water, which allows

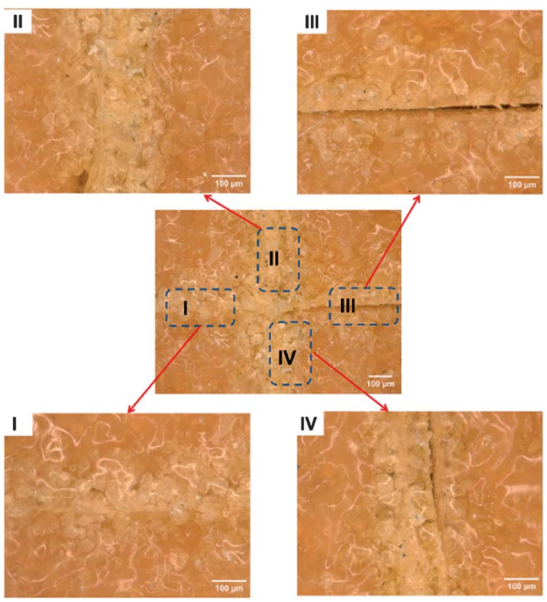

Fig. 7 Different scratch widths and numbers of scratch repeats influencing the self-healing phenomenon on the copper surface. Area (I): one scratch (10 μm scratch width). Area (II) and (IV): two consecutive scratches (each 10 μm). Area (III): one scratch (30 μm scratch width).

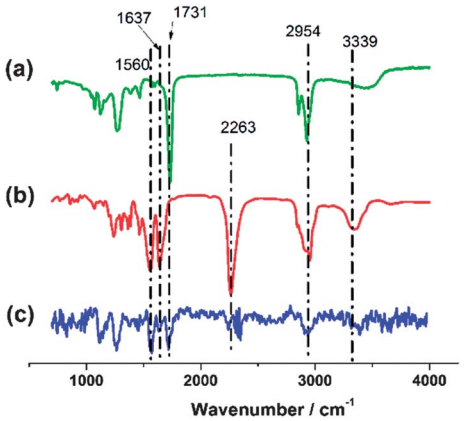

Fig. 8 FT-IR spectra of the AVC (a), polyurethane (b), and self-healing materials in the crevice (c), respectively.

electrochemical reactions between the metal and the seawater. A potential distribution map of the steel surface can be obtained by measuring potential differences between a scanning microprobe and a micro-reference electrode[26] (Fig. 9). After 12 h of immersion, the potential difference of an AVC-coated metal was larger compared to an IPDI-AVC coated sample. As the AVC has no self-healing ability, the corrosion area of the crevice became larger after immersion for 12 h (Fig. 9a–c).

However, after 12 h of immersion, the potential difference along the scratched crevice decreased when IPDI-AVC was used as the coating (Fig. 9d–f). The IPDI from microcapsules healed the crevice and isolated the metal substrate from the NaCl solution. Thus, SMRE could not obtain the potential difference signal, as shown in Fig. 9f. Furthermore, the potential difference range of scratched IPDI-AVC (from −0.78 to 0.78 mV) is obviously smaller than that of scratched neat AVC (from −1.04 to 1.04 mV), indicating that the IPDI from the microcapsules

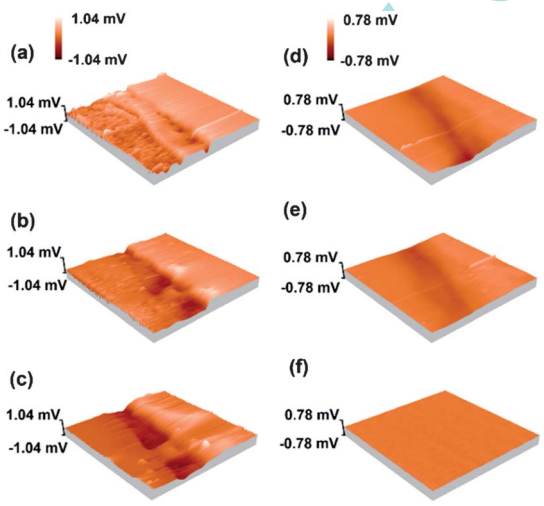

Fig. 9 Potential distributions above scratched Q235 steel substrates covered with AVC (a–c) and IPDI-AVC (d–f) measured by SMRE (2 mm × 2 mm). (a and d) Correspond to 0.5 h of immersion, (b and e) to 4 h of immersion, and (c and f) to 12 h of immersion in 0.01 M NaCl solution. The potential was measured 10 μm above the sample surface.

could gradually form the solid to reduce the potential difference caused by metal corrosion.

Self-healing mechanism

Fig. 10 shows a schematic depiction of the successive events after scratching of the AVC to expose the substrate, followed by immersion in seawater (Fig. 10a). After a deep scratch in the self-healing coating, two side walls of the crevice touch each other due to the AVC's elasticity. Seawater cannot directly penetrate into the bottom of the crevice (Fig. 10b). During a short immersion time, seawater penetrates into the mouth of the crevice, where water triggers the inflow of self-healing materials from the microcapsules (Fig. 10c). Healing materials mix and react with seawater, and reaction products fill with the bottom and walls of the crevice (Fig. 10d). Since the scratch now has an open gap, seawater can continue to penetrate into the healed crevice down to the metal bottom (Fig. 10e). Healing materials from the microcapsules along the re-penetrated crevice also have the ability to heal the scratch (Fig. 10f). Additionally, the IPDI microcapsules have swelling properties.[27] The two previous steps can be repeated up to three or four times, thereby creating an efficient multi-self-healing process. Seawater that penetrates into the AVC causes microcapsule swelling[24] (Fig. 10g). The swelling phenomenon leads to cracks in the microcapsules, which is a necessary factor for the flow of healing materials from the microcapsule core to the seawater path and crevice. The healing materials along the flow path will again create a barrier against seawater penetration (Fig. 10h). Steps (g) and (h) can occur repeatedly until the reactions run out of substrates.

EIS characterization

EIS was used to monitor the self-healing process.[28] An initial equivalent electrical circuit (EEC) was used for the data analysis of the self-healing process of the damaged coatings (Fig. 11). All the EIS tests were performed at a temperature of 30 °C.

Nyquist plots show the typical analytical method of EIS. An elimination of the equivalent electrical circuit leads to:[29] $\left[Z_{re} - \left(R_s + \frac{1}{2}R_c\right)\right]^2 + (Z_{im})^2 = \left(\frac{R_c}{2}\right)^2$ The maximum height of the $-Z_{im}$ for each Nyquist plot corresponds to a circle with a

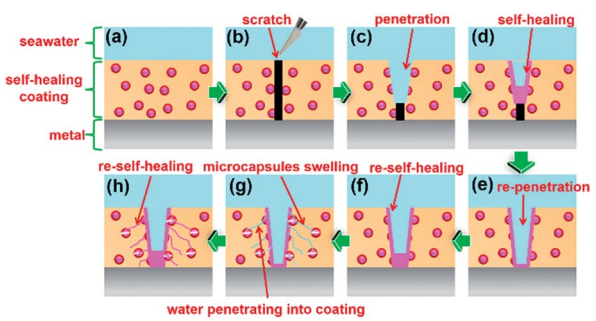

Fig. 10 Flow chart of the self-healing mechanism of the AVC after repeated scratching.

radius of $R_c/2$ of the equation. Therefore, Nyquist plots (Fig. 12a–c) can be used to correspondingly monitor the self-healing process of the coating.

In Fig. 12, the magenta lines show that the value of $R_c/2$ decreases from 19.096 to 2.477 MΩ cm^2 after the scratched sample was dipped into seawater for 8 h. The decreasing trend of the magenta line indicates the penetration of seawater into the mouth of the crevice, according to the mechanism shown in Fig. 10b and c. The red, green and blue colors respectively show the peak, the trough and the transition stages of the self-healing process of the scratch coating.

Before 100 h (Fig. 12b), the healing process follows the mechanism of Fig. 10d–f. Processes depicted in Fig. 10e and f can occur repeatedly until all healing materials have reacted along the walls of the crevice.

After 100 h, the seawater started to penetrate into the coating from the walls of the scratch. Exposure of the microcapsules to seawater causes swelling of the shells of the microcapsules, which in turn causes healing materials to flow out of the microcapsules, sequentially filling the seawater path and the scratched crevice. Meanwhile, healing materials react with seawater to heal the path of the seawater penetration and the scratched crevice.

When there are not enough microcapsules left to provide enough materials for complete healing, or if the seawater cannot achieve microcapsule swelling due to coating protection, the AVC loses the ability to self-heal, and cannot resist seawater penetration. Nyquist plots of such coating failures are shown in purple in Fig. 12c.

The total resistance combination ($R_s + R_c + R_{ct}$) of the Bode plot of EIS effectively showed the protective properties of the coating to the metal body.[30] The impedance modulus ($|Z|$) of each Bode plot, at a frequency of 0.01 Hz[31], was used for the evaluation of coating resistance in Fig. 12d–f. Four typical parts of the impedance modulus value (f = 0.01 Hz) in the curve could be distinguished. Parts (I), (II), (III) and (IV) of Fig. 12e corresponded to seawater penetrating into crevice, the self-healing process along the crevice, the self-healing process of seawater penetrating into coating, and failure of the coating, respectively.

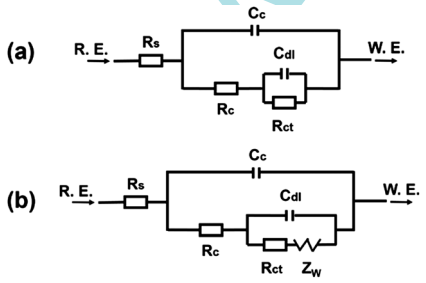

Fig. 11 Electrical equivalent circuit models for scratched IPDI-AVC coated surfaces (a) and in the presence of diffusion (b). (R.E.: reference electrode, W.E.: working electrode, C_c: coating capacitance (F cm^{-2}), C_{dl}: metal double layer capacitance (F cm^{-2}), R_s: solution resistance (Ω cm^2), R_c: coating resistance (Ω cm^2), R_{ct}: metal charge transfer resistance (Ω cm^2), Z_W: Warburg diffusion coefficient (Ω cm^2).)

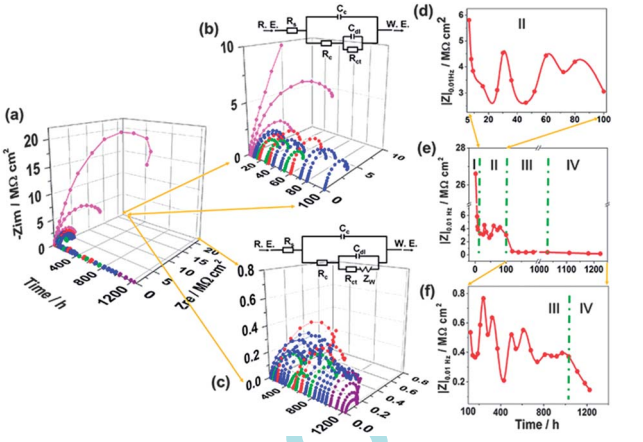

Fig. 12 (a) Nyquist plots of 5083 aluminum (1 cm × 1 cm) coated with IPDI-AVC with a 0.5 cm length scratch. The different color lines represent different corrosion stages. Magenta: start; red: peak; blue: transition stage; green: trough; purple: coating failure. (b) Nyquist curves of 5083 aluminum IPDI self-healing coating dipped into seawater before 100 h (b) and after 100 h (c). Impedance modulus (f = 0.01 Hz) of the coating in seawater from 6.5 h to 100 h (d), from 0.5 h to 1224 h (e), and from 120 h to 1224 h (f).

The $|Z|$ value decreased in parts (I) and (IV) of the curve, while, the $|Z|$ value fluctuated in parts (II) and (III), demonstrating the on-going self-healing process. However, the $|Z|$ value in part (II) is nearly six times higher than the $|Z|$ value in part (III), providing evidence for the mechanism detailed in of Fig. 10e–h. Neat AVC without IPDI microcapsules on the 5083 aluminum surface had no self-healing properties as shown in Fig. 13. The $|Z|$ value of neat AVC decreased to less than 0.06 MΩ cm^2 within 5 h immersion.

Fig. 13 shows the $|Z|$ value of scratched neat AVC without IPDI microcapsules on a 5083 aluminum surface immersed in seawater. After the seawater penetrated into the 5083 aluminum surface, the impedance of the coating could not increase to protect 5083 aluminum due to the neat AVC without self-healing ability.

Self-healing ability on different metal substrates

Fig. 14 shows that the $|Z|$ value of IPDI-AVC on a titanium surface immersed in seawater could keep a relative high impedance with slight fluctuations due to the self-healing

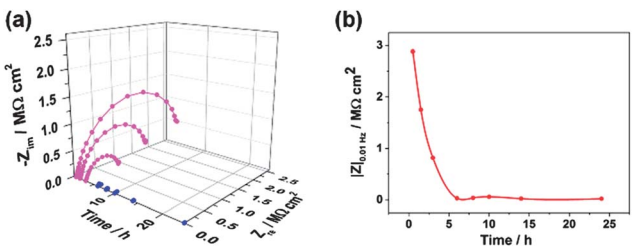

Fig. 13 Nyquist plots (a) and impedance modulus (f = 0.01 Hz) (b) of the scratched neat AVC without IPDI microcapsules on the 5083 aluminum surface, immersed in seawater.

process. The $|Z|$ value fluctuates many times from 200 to 750 h of immersion, indicating that the self-healing process occurs in this stage coupled with seawater penetration and coating failure. Moreover, the $|Z|$ value of IPDI-AVC on the titanium surface is higher than that on the 5083 aluminum surface at the same immersion time. This phenomenon proved that the IPDI-AVC had better self-healing ability on the titanium substrate than on the 5083 aluminum. The scratched crevice was well healed after 200 h (Fig. 14e) and 1200 h (Fig. 14f) of immersion.

For the copper substrate, the IPDI-AVC has the same self-healing ability and different self-healing stages as shown in Fig. 15. The self-healing process is represented by the $|Z|$ value. However, the self-healing ability of the coated copper surface could not be maintained for more than 450 h, which is less than that on 5083 aluminum (>1000 h) and titanium (>1000 h).

The $|Z|$ value of IPDI-AVC on the Q235 surface decreased to less than 0.06 MΩ cm^2 within 330 h of immersion as shown in Fig. 16. It proved that out of the four metal substrates, the IPDI-AVC on the Q235 surface maintained the self-healing ability for the shortest time. The self-healing time was also influenced by the width of the scratched crevice that was described in Fig. 7. Although the scratched crevice was healed after immersion, the seawater could penetrate into the Q235 substrate, causing corrosion products after 500 h immersion. There were red corrosion products in the crevice in Fig. 16f.

Thus, the self-healing time of IPDI-AVC depended on the different metal substrates. The self-healing process was slower

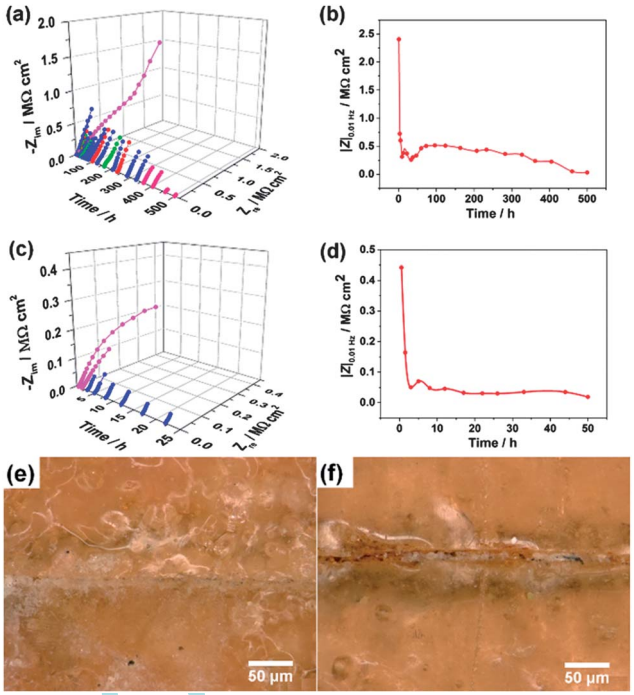

Fig. 15 Nyquist plots (a and c) and impedance modulus ($f = 0.01$ Hz) (b and d) of the IPDI-AVC (a and b) and the scratched neat AVC without IPDI microcapsules (c and d) on the copper surface immersed in seawater, respectively. Scratched IPDI-AVC on the copper surface immersed in seawater after 400 h (e) and 600 h (f).

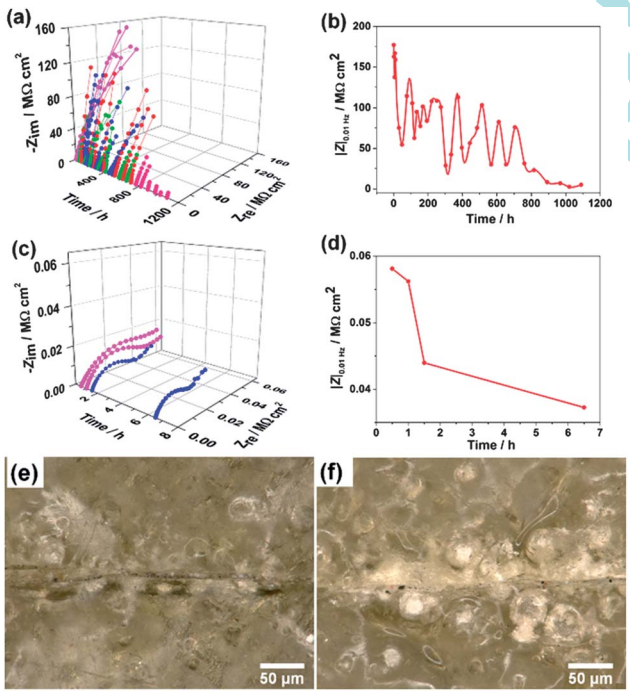

Fig. 14 Nyquist plots (a and c) and impedance modulus ($f = 0.01$ Hz) (b and d) of the IPDI-AVC (a and b) and the scratched neat AVC without IPDI microcapsules (c and d) on the titanium surface immersed in seawater, respectively. Scratched IPDI-AVC on titanium surface immersed in seawater after 200 h (e) and 1200 h (f). The different colored lines are defined in Fig. 12.

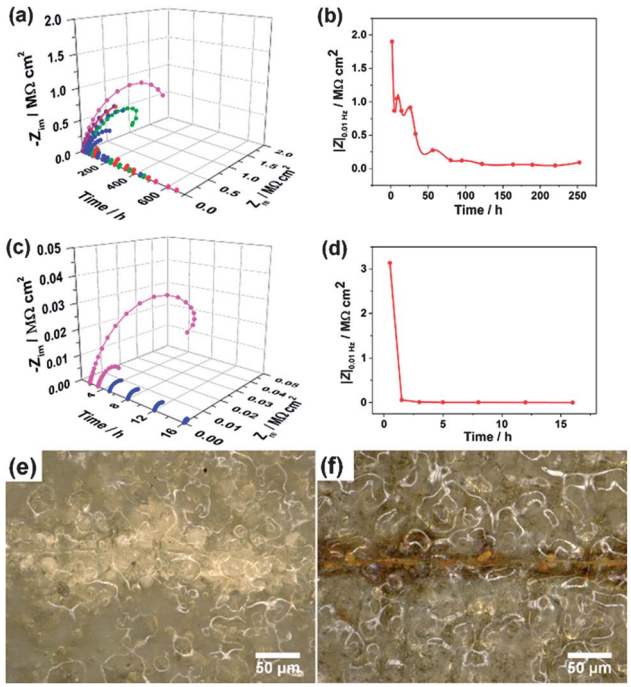

Fig. 16 Nyquist plots (a and c) and impedance modulus ($f = 0.01$ Hz) (b and d) of the IPDI-AVC (a and b) and the scratched neat AVC without IPDI microcapsules (c and d) on the Q235 surface immersed in seawater, respectively. Scratched IPDI-AVC on the Q235 surface immersed in seawater after 200 h (e) and 500 h (f).

when using active metal substrates such as Q235 steel, while the influence was less in metals that had a thin oxide layer such as the 5083 aluminum, titanium or copper substrates.

Conclusions

In conclusion, a new self-healing coating was prepared by adding isocyanate microcapsules as functional additives to AVC. A mechanistic model of the self-healing process of the AVC over a metal surface was established, which was evidenced by EIS and SMRE. Our results are clearly different from the results obtained with the self-healing coating with microcapsules as functional self-healing materials, where the impedance modulus decreased continuously in the solution.[32] This functional AVC has advantages for self-healing materials with microvascular networks, yet they are thin enough to be suitable for a wide range of applications with simple preparation.

Acknowledgements

This work was supported by the China Postdoctoral Science Foundation (no. 2013M531686).

Notes and references

1 (*a*) M. M. Caruso, D. A. Davis, Q. Shen, S. A. Odom, N. R. Sottos, S. R. White and J. S. Moore, *Chem. Rev.*, 2009, **109**, 5755; (*b*) D. G. Shchukin and H. Möhwald, *Chem. Commun.*, 2011, **47**, 8730.

2 Y. González-García, J. M. C. Mol, T. Muselle, I. De Graeve, G. Van Assche, G. Scheltjens, B. Van Mele and H. Terryn, *Electrochim. Acta*, 2011, **56**, 9619.

3 S. J. Pastine, D. Okawa, A. Zettl and J. M. J. Fréchet, *J. Am. Chem. Soc.*, 2009, **131**, 13586.

4 (*a*) M. Huang, H. Zhang and J. Yang, *Corros. Sci.*, 2012, **65**, 561; (*b*) S. H. Cho, S. R. White and P. V. Braun, *Adv. Mater.*, 2009, **21**, 645.

5 S. J. García, H. R. Fischer and S. van der Zwaag, *Prog. Org. Coat.*, 2011, **72**, 211.

6 A. P. Esser-Kahn, N. R. Sottos, S. R. White and J. S. Moore, *J. Am. Chem. Soc.*, 2010, **132**, 10266.

7 (*a*) S. R. White, N. R. Sottos, P. H. Geubelle, J. S. Moore, M. R. Kessler, S. R. Sriram, E. N. Brown and S. Viswanathan, *Nature*, 2001, **409**, 794; (*b*) E. N. Brown, S. R. White and N. R. Sottos, *J. Mater. Sci.*, 2004, **39**, 1703.

8 J. Fickert, P. Rupper, R. Graf, K. Landfester and D. Crespy, *J. Mater. Chem.*, 2012, **22**, 2286.

9 Y.-K. Song, Y.-H. Jo, Y.-J. Lim, S.-Y. Cho, H.-C. Yu, B.-C. Ryu, S.-I. Lee and C.-M. Chung, *ACS Appl. Mater. Interfaces*, 2013, **5**, 1378.

10 X. Hao, H. Liu, Z. Lu, Y. J. Xie and H. Y. Yang, *J. Mater. Chem. A*, 2013, **1**, 6920.

11 R. Tian, X. L. Fu, Y. D. Zheng, X. Liang, Q. L. Wang, Y. Ling and B. S. Hou, *J. Mater. Chem.*, 2012, **22**, 25437.

12 M. L. Zheludkevich, J. Tedim, C. S. R. Freire, S. C. M. Fernandes, S. Kallip, A. Lisenkov, A. Gandini and M. G. S. Ferreira, *J. Mater. Chem.*, 2011, **21**, 4805.

13 (*a*) J. Yang, M. W. Keller, J. S. Moore, S. R. White and N. R. Sottos, *Macromolecules*, 2008, **41**, 9650; (*b*) M. X. Huang and J. L. Yang, *J. Mater. Chem.*, 2011, **21**, 11123.

14 (*a*) C. J. Hansen, S. R. White, N. R. Sottos and J. A. Lewis, *Adv. Funct. Mater.*, 2011, **21**, 4320; (*b*) J. D. Rule, E. N. Brown, N. R. Sottos, S. R. White and J. S. Moore, *Adv. Mater.*, 2005, **17**, 205.

15 J. Fox, J. J. Wie, B. W. Greenland, S. Burattini, W. Hayes, H. M. Colquhoun, M. E. Mackay and S. J. Rowan, *J. Am. Chem. Soc.*, 2012, **134**, 5362.

16 (*a*) E. Gonzalez, J. Pavez, I. Azocar, J. H. Zagal, X. Zhou, F. Melo, G. E. Thompson and M. A. Páez, *Electrochim. Acta*, 2011, **56**, 7586; (*b*) D. G. Shchukin, S. V. Lamaka, K. A. Yasakau, M. L. Zheludkevich, M. G. S. Ferreira and H. Möhwald, *J. Phys. Chem. C*, 2008, **112**, 958; (*c*) S. Neema, M. Selvaraj, J. Raguraman and S. J. Ramu, *J. Appl. Polym. Sci.*, 2013, **127**, 740.

17 S. V. Lamaka, M. L. Zheludkevich, K. A. Yasakau, R. Serra, S. K. Poznyak and M. G. S. Ferreira, *Prog. Org. Coat.*, 2007, **58**, 127.

18 W. Wang, L. Xu, F. Liu, X. Li and L. Xing, *J. Mater. Chem. A*, 2013, **1**, 776.

19 R. van Gorkum and E. Bouwman, *Coord. Chem. Rev.*, 2005, **249**, 1709.

20 S. W. Kim, T. Kim, Y. S. Kim, H. S. Choi, H. J. Lim, S. J. Yang and C. R. Park, *Carbon*, 2012, **50**, 3.

21 (*a*) N. Bialas and H. Höcker, *Makromol. Chem.*, 1990, **191**, 1843; (*b*) A. Prabhakar, D. K. Chattopadhyay, B. Jagadeesh and K. V. S. N. Raju, *J. Polym. Sci., Part A: Polym. Chem.*, 2005, **43**, 1196.

22 E. Delebecq, J.-P. Pascault, B. Boutevin and F. Ganachaud, *Chem. Rev.*, 2013, **113**, 80.

23 M. M. Caruso, B. J. Blaiszik, S. R. White, N. R. Sottos and J. S. Moore, *Adv. Funct. Mater.*, 2008, **18**, 1898.

24 H. Masoud and A. Alexeev, *ACS Nano*, 2012, **6**, 212.

25 (*a*) N. Cui, H. Y. Ma, J. L. Luo and S. Chiovelli, *Electrochem. Commun.*, 2001, **3**, 716.

26 (*a*) H. Xu, Y. Liu, W. Chen, R.-G. Du and C.-J. Lin, *Electrochim. Acta*, 2009, **54**, 4067; (*b*) B. Lin, R. Hu, C. Ye, Y. Li and C. Lin, *Electrochim. Acta*, 2010, **55**, 6542.

27 T. Dobashi, T. Furukawa, K. Ichikawa and T. Narita, *Langmuir*, 2002, **18**, 6031.

28 (*a*) P. L. Bonora, F. Deflorian and L. Fedrizzi, *Electrochim. Acta*, 1996, **41**, 1073; (*b*) J. B. Jorcin, G. Scheltjens, Y. Van Ingelgem, E. Tourwé, G. van Assche, I. de Graeve, B. van Mele, H. Terryn and A. Hubin, *Electrochim. Acta*, 2010, **55**, 6195.

29 F. Mansfeld, M. W. Kendig and S. Tsai, *Corrosion*, 1982, **38**, 570.

30 G. W. Walter, *Corros. Sci.*, 1986, **26**, 681.

31 J. B. Cambon, F. Ansart, J. P. Bonino and V. Turq, *Prog. Org. Coat.*, 2012, **75**, 486.

32 (*a*) H. Choi, Y. K. Song, K. Y. Kim and J. M. Park, *Surf. Coat. Technol.*, 2012, **206**, 2354; (*b*) D. Borisova, H. Möhwald and D. G. Shchukin, *ACS Appl. Mater. Interfaces*, 2012, **4**, 2931.